Acta Pharmaceutica Sinica B 2022;12(5):2224–2238

Chinese Pharmaceutical Association
Institute of Materia Medica, Chinese Academy of Medical Sciences

Acta Pharmaceutica Sinica B

www.elsevier.com/locate/apsb
www.sciencedirect.com

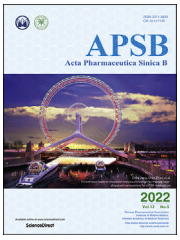

ORIGINAL ARTICLE

Crosstalk between CYP2E1 and PPARα substrates and agonists modulate adipose browning and obesity

Youbo Zhang[a,b,†], Tingting Yan[b,*,†], Tianxia Wang[a,c], Xiaoyan Liu[a], Keisuke Hamada[b], Dongxue Sun[b], Yizheng Sun[a], Yanfang Yang[a], Jing Wang[a], Shogo Takahashi[b], Qiong Wang[b], Kristopher W. Krausz[b], Changtao Jiang[d], Cen Xie[b], Xiuwei Yang[a,*], Frank J. Gonzalez[b,*]

[a]*State Key Laboratory of Natural and Biomimetic Drugs and Department of Natural Medicines, School of Pharmaceutical Sciences, Peking University, Beijing 100191, China*
[b]*Laboratory of Metabolism, Center for Cancer Research, National Cancer Institute, National Institutes of Health, Bethesda, MD 20892, USA*
[c]*School of Life Science and Engineering, Lanzhou University of Technology, Lanzhou 730050, China*
[d]*Department of Physiology and Pathophysiology, School of Basic Medical Sciences, Peking University, the Key Laboratory of Molecular Cardiovascular Science, Ministry of Education, Beijing 100191, China*

Received 18 November 2021; received in revised form 11 January 2022; accepted 28 January 2022

KEY WORDS

CYP2E1;
PPARα;
FGF21;
Metabolic enzyme;
Nuclear receptor;
Obesity

Abstract Although the functions of metabolic enzymes and nuclear receptors in controlling physiological homeostasis have been established, their crosstalk in modulating metabolic disease has not been explored. Genetic ablation of the xenobiotic-metabolizing cytochrome P450 enzyme CYP2E1 in mice markedly induced adipose browning and increased energy expenditure to improve obesity. CYP2E1 deficiency activated the expression of hepatic peroxisome proliferator-activated receptor alpha (PPARα) target genes, including fibroblast growth factor (FGF) 21, that upon release from the liver, enhanced adipose browning and energy expenditure to decrease obesity. Nineteen metabolites were increased in *Cyp2e1*-null mice as revealed by global untargeted metabolomics, among which four compounds, lysophosphatidylcholine and three polyunsaturated fatty acids were found to be directly metabolized by CYP2E1 and to serve as PPARα agonists, thus explaining how CYP2E1 deficiency causes hepatic PPARα activation through increasing

*Corresponding authors.
E-mail addresses: xwyang@bjmu.edu.cn (Xiuwei Yang), tingting.yan@nih.gov (Tingting Yan), gonzalef@mail.nih.gov (Frank J. Gonzalez).
†These authors made equal contributions to this work.
Peer review under responsibility of Chinese Pharmaceutical Association and Institute of Materia Medica, Chinese Academy of Medical Sciences.

https://doi.org/10.1016/j.apsb.2022.02.004

cellular levels of endogenous PPARα agonists. Translationally, a CYP2E1 inhibitor was found to activate the PPARα−FGF21−beige adipose axis and decrease obesity in wild-type mice, but not in liver-specific *Ppara*-null mice. The present results establish a metabolic crosstalk between PPARα and CYP2E1 that supports the potential for a novel anti-obesity strategy of activating adipose tissue browning by targeting the CYP2E1 to modulate endogenous metabolites beyond its canonical role in xenobiotic-metabolism.

1. Introduction

Obesity and the associated metabolic disorders are increasing at an alarming rate globally, particularly in Western countries[1]. An imbalance between energy intake and expenditure results in obesity, and activation of adipose browning, characterized in rodent models, is an attractive strategy for enhancing non-shivering thermogenesis and thus countering the excess energy intake[2]. When voluntary lifestyle and dietary strategies fail, medical treatment becomes a necessary means for the treatment of obesity. However, no effective pharmacotherapies are available in the clinic.

Glucolipid-metabolic enzymes and nuclear receptors have become drug targets for the treatment of obesity[3,4], although less is known about their roles in the modulation of adipose browning. Cytochrome P450 (CYP) 2E1 was suggested to be closely related to the pathological process of metabolic diseases. CYP2E1 activity is significantly increased in both humans and experimental rodent models under conditions of diabetes[5], fasting[6], obesity[7], and high-fat diet (HFD) treatment[8]. *Cyp2e1*-null mice are protected from HFD-induced obesity[9] and nonalcoholic steatohepatitis[10]. Peroxisome proliferator-activated receptor alpha (PPARα) plays an essential role in lipid homeostasis and energy regulation, and the expression and excretion of hepatic fibroblast growth factor (FGF)21[11], a major PPARα target gene in liver[12], could act as an endocrinal beige stimulator to alleviate the obesity[13]. However, the mechanism by which CYP2E1 affects metabolic diseases has not been explored.

CYP2E1 was initially identified as an ethanol-inducible enzyme[14] involved in the metabolism of various low-molecular weight xenobiotics including ethanol, benzene, carbon tetrachloride, and acetaminophen[15]. Notably beyond these xenobiotics, CYP2E1 also metabolizes endogenous substrates including fatty acids[16−20], while various endogenous ligands, also including fatty acids, were reported to activate PPARα[21−23]. Thus, it is possible that some of the endogenous substrates of CYP2E1 also serve as PPARα agonists. However, how the shared substrates and ligands of CYP2E1 and PPARα could act as signal-transducing molecules in modulating metabolic diseases are largely unknown.

In the present study, to explore the potential crosstalk between CYP2E1 and PPARα, global genomics, metabolomics in combination with *Cyp2e1*-null mice and liver-specific *Ppara*-null mice ($Ppara^{\Delta Hep}$) as well as the CYP2E1 inhibitor diethyldithiocarbamate (DDC)[24] were employed to uncover the mechanism by which CYP2E1 deficiency decreases obesity.

2. Materials and methods

2.1. Chemicals and reagents

DDC, docosahexaenoic acid (DHA), arachidonic acid (AA), 9,12-linoleic acid (LCA), and Wy-14643 were purchased from Sigma−Aldrich (Saint Louis, MI, USA). Lipofectamine 3000 was obtained from Invitrogen (Carlsbad, CA, USA). Human pGST-PPARα and X3-TK-PPRE-luciferase vectors were from Addgene (Watertown, MA, USA). The pCMV-renilla luciferase vector was provided by Grace L. Guo (Rutgers University, New Brunswick, NJ, USA). Mouse/rat FGF21 quantitative enzyme-linked immunosorbent assay kit was purchased from R&D systems (Minneapolis, MN, USA). Anti-uncoupling protein 1 (UCP1) primary antibody (ab209483) and HRP-conjugated goat anti-rabbit IgG were obtained from Abcam (Cambridge, UK). Primers were ordered from Integrated DNA Technologies (San Diego, CA, USA). HEK-293 cells were purchased from American Type Culture Collection (ATCC, Manassas, VA, USA).

2.2. Animal treatment

Eight-week-old male *Cyp2e1*-null[25] and wild-type (WT) mice on the 129/SVJ background were used. The mice were fed a 60% HFD (S3282, Bioserv, New Brunswick, NJ, USA) for 14 weeks. To test the therapeutic effect of DDC in WT and $Ppara^{\Delta Hep}$ mice[26], eight-week-old male mice were randomly divided into two groups ($n = 6$ mice per group), maintained on HFD feeding and intraperitoneally administered phosphate buffered saline (PBS) for the control group or DDC at a dose of 40 mg/kg once a day starting from the first day of HFD feeding, for eight consecutive weeks. This dose of DDC was determined based on pilot studies of 10 mg/kg and 40 mg/kg revealing that 40 mg/kg had an anti-obesity effect with no overt hepatic toxicity. For all HFD feeding studies, the weights were recorded once a week. The Peking University Committee on Animal Care and Use (SYXK [Jing]2006-0025) and the National Cancer Institute Animal Care and Use Committee approved all animal protocols used in this study.

2.3. Glucose tolerance test and insulin tolerance test

After 10 weeks of HFD feeding, glucose tolerance tests (GTT) and insulin tolerance tests (ITT) were carried out after fasting for 16 h (for GTT) or 6 h (for ITT) using a glucometer to measure the glucose levels from blood taken from tails (Bayer, Pittsburgh, PA, USA) following intraperitoneal injection with glucose (2 g/kg) or insulin (0.8 U/kg; Eli Lilly, Indianapolis, IN, USA). ITT was performed one week after the GTT. Tail blood was collected at the indicated time right before or after intraperitoneal injection of glucose (for GTT) or insulin (for ITT) in 2.5 h.

2.4. Body composition and indirect calorimetry

An EchoMRI 3-in-1 mouse scanner (EchoMRI, Houston, TX, USA) was used to determine body fat and lean mass of live mice

following the manufacturer's protocol. Indirect calorimetry was carried out on mice using an Environment Controlled CLAMS (Columbus Instruments, Columbus, OH, USA). Spontaneous locomotor activity, energy expenditure, oxygen consumption (VO_2) and carbon dioxide production (VCO_2) were determined as previously described[27].

2.5. Lipid analysis

Serum and liver triglycerides (TG) and total cholesterol (TC) were determined with assay kits obtained from Wako Chemicals (Richmond, VA, USA), respectively. Serum alanine transaminase (ALT) and aspartate aminotransferase (AST) levels were measured using a standard automatic analyzer or a commercial ALT or AST assay kit (Catachem, Bridgeport, CT, USA).

2.6. Surface plasmon resonance

Surface plasmon resonance (SPR) assays were carried out on a Biacore T200 instrument (GE Healthcare, Chicago, IL, USA) according to the protocol provided by GE Healthcare to test if DHA, AA, and LCA could directly bind to the PPARα protein. Recombinant human PPARα protein with an N-terminal His Tag was immobilized on CM5 chip (GE Healthcare, Chicago, IL, USA) through 1-ethyl-3-(3′-dimethylaminopropyl) carbodiimide/*N*-hydroxysuccinimide (EDC/NHS)-mediated crosslinking reaction. The peptide sequence of the PPARα protein is described in Supporting Information Table S1. The three polyunsaturated fatty acids (PUFAs) (DHA, AA and LCA) were used at concentrations ranging from 1.56 to 50 μmol/L. Each analysis was repeated three times to confirm the stability of the sensor surface. The parameters of SPR were as follows: contact time, 60 s; disassociation time, 150 s; flow rate, 30 μL/min; temperature, 25 °C. A steady-state affinity model was performed for affinity curve fitting and the disassociation constant K_d was calculated with Biacore T200 Evaluation Software (Version 1.0).

2.7. Molecular docking in silico

To evaluate the possible binding mode of DHA, AA, and LCA to PPARα as potential ligands, the human PPARα-ligand binding domain [Protein Data Bank (PDB): 5AZT] was selected as described in a previous study[28]. Molecular docking analyses of DHA, AA, and LCA to PPARα were performed with GOLD 5.2.2 software.

2.8. Luciferase reporter assays

For the luciferase reporter gene assays, HEK-293 cells were seeded into 24-well plates at 1×10^4/well for 12 h. The plasmids (human pGST-PPARα plasmid, X3-TK-PPRE-luciferase vector, and pCMV-renilla luciferase vector) were co-transfected using Lipofectamine 3000 reagent. After transfection for 24 h, the cells were treated with 10 μmol/L of Wy-14643, DHA, AA, and LCA or 5 or 10 μmol/L of LysoPC 22:4 for 24 h, respectively. The selected doses of LysoPC 22:4 were found to be nontoxic using pilot cell toxicity studies. Luciferase activity was measured with Dual-Luciferase Reporter Assay System (Promega, Madison, WI, USA). *Renilla* luciferase activity was utilized to normalize the transfection efficiency.

2.9. Enzyme incubation studies

In vitro metabolism studies for DDC inhibition and recombinant enzyme incubations were performed as described previously[29,30]. In brief, the incubation system (200 μL) contained 50 mmol/L Tris−HCl buffer solution (pH = 7.4), 5 mmol/L $MgCl_2$, 0.5 mg/mL human liver microsomes, 10 μmol/L of substrates dissolved in 0.1% dimethylsulfoxide and 1 mmol/L NAPDH. After 30 min incubation at 37 °C, the reactions were terminated with 200 μL cold aqueous acetonitrile containing 5 μmol/L chlorpropamide. For the DDC inhibition study, DDC was used at 20 μmol/L and preadded to the incubation system.

2.10. Quantitative real-time polymerase chain reaction

RNA was extracted from frozen tissues including liver, brown adipose tissue (BAT), subcutaneous white adipose tissue (SWAT) and epididymal white adipose tissue (EWAT) by using TRIzol reagent (Invitrogen, Carlsbad, CA, USA). cDNA was synthesized from 1 μg of total RNA using qScript™ cDNA SuperMix (Quantabio, Beverly, MA, USA). All primer sequences for quantitative real-time polymerase chain reaction (qPCR) are listed in Supporting Information Table S2. qPCR was performed on an ABI 7900HT Fast Real-Time PCR System using SYBR Green PCR master mix (AB Applied Biosystems, Warrington, UK). Relative mRNA levels were calculated after normalizing to corresponding *Actb* mRNA and the results expressed as fold change relative to the control group.

2.11. Serum FGF21 assay

A mouse/rat FGF21 quantitative enzyme-linked immunosorbent assay kit was used to determine serum FGF21 levels following the manufacturer's protocol.

2.12. Histopathology assessment and immunohistochemistry

Liver and adipose tissues were cut and immediately fixed in 4% paraformaldehyde for 24 h at room temperature, dehydrated and embedded in paraffin. Then, the tissues were sectioned into thick slices (4 mm) and stained with hematoxylin and eosin (H&E). For immunohistochemistry, SWAT were processed as described previously[27] with rabbit polyclonal anti-UCP1 primary antibody and horseradish peroxidase-conjugated goat anti-rabbit IgG. Slide digital images were collected at 400 times magnification with Pannoramic Viewer software (v.1.15.2, 3DHISTECH Ltd, Budapest, Hungary). Images shown were representative results of three biological replicates.

2.13. Transcriptome analysis

After feeding a HFD for 14 weeks, the liver samples were randomly selected for RNA-seq (n = 3 for each group). Liver tissue samples were homogenized, and total RNA was extracted using the Qiagen miRNeasy mini kit (Qiagen, Hilden, Germany) according to the manufacturer's instructions. An Agilent 2100 Bioanalyzer and a Nanodrop was used for determination of the isolated RNA quantity and quality. cDNA libraries were constructed using an Illumina TruSeq RNA LS Sample Preparation kit v2 (Illumina, San Diego, CA, USA). Final individual cDNA libraries were assessed for fragment size and quality with the 2100 Bioanalyzer (Agilent, Santa Clara, CA, USA) and sequencing

libraries were quantified with the ABI StepOnePlus Real-Time PCR System (Thermo Fisher, Waltham, MA, USA). Paired terminal sequencing was performed on an HiSeq 2500 sequencer (Illumina, San Diego, CA, USA). Differential expression analysis was performed according to the gene expression in different sample groups. GO functional analysis, pathway functional analysis, cluster analysis, and gene−gene interaction network analysis were used to analyze the differentially expressed genes. Transcriptomic data were deposited in the Gene Expression Omnibus under accession code GSE193796.

2.14. LC−MS/MS-based metabolomics

Sample preparation and metabolomics analyses of livers were as described[31]. Sample analyses were performed on an ultra-performance liquid chromatography coupled Xevo G2 quadrupole time-of-flight mass spectrometer with an ACQUITY UPLC and a Waters Acquity CSH 1.7-μm C18 column (2.1 mm × 100 mm; Waters, Milford, MA, USA).

2.15. Synthesis of LysoPC 22:4

To synthesize LysoPC 22:4, *cis*-7,10,13,16-docosatetraenoic acid (SM1) and choline glycerophosphate (SM2) were selected as the synthetic materials (see Fig. 4). At the first step, the corresponding chloride of SM1 was obtained. Acyl chloride was generated from the reaction of SM1 with oxalyl chloride in the presence of anhydrous *N*,*N*-dimethylformamide catalyst under moderate reaction conditions from 0 °C to room temperature. Then, the reaction of SM2 and acyl chloride yielded LysoPC 22:4 in good yields (66%) with two steps. The first step was carried out with reflux for 1 h using Bu_2SnO as a catalyst. LysoPC 22:4 was finally synthesized at room temperature in isopropanol (*i*PrOH) in the presence of triethylamine (Et_3N). The chemical structure of LysoPC 22:4 was confirmed by nuclear magnetic resonance and mass spectroscopy.

2.16. Statistical analysis

The values are expressed as mean ± standard error of mean (SEM). Statistic difference was determined by two-tailed student's *t*-test between two groups or one-way ANOVA followed by Bonferroni posttest among multiple comparisons using Prism version 7.0 (GraphPad Software, San Diego, CA, USA). A value of $P < 0.05$ was considered statistically significant.

3. Results

3.1. CYP2E1 deficiency induces adipose browning and enhances energy expenditure to improve obesity

To examine the role of CYP2E1 in modulating obesity, WT and *Cyp2e1*-null mice were subjected to HFD feeding for 14 weeks to induce obesity. Consistent with previous findings that *Cyp2e1*-null mice were resistant to HFD-induced obesity[9], the *Cyp2e1*-null mice gained less body weight (Supporting Information Fig. S1A), had improved insulin sensitivity (Fig. S1B and S1C) and showed decreased serum ALT, AST and TC levels without significant changes in serum TG levels (Fig. S1D−S1G) compared to WT mice. No differences in food intake and activity were found between *Cyp2e1*-null mice and WT mice (Fig. S1H and S1I). However, body composition analysis showed that the weight gain in WT mice was mainly due to an increase in adipose tissue mass compared to the *Cyp2e1*-null mice, and the lean mass of the *Cyp2e1*-null mice was even higher than that of WT mice (Fig. 1A). Consistently, the mass of SWAT and EWAT in WT mice were higher than that of *Cyp2e1*-null mice (Fig. 1B). Rectal temperatures of the WT and *Cyp2e1*-null mice were then measured under chow diet or after 14 weeks of HFD. Under chow diet, the basal rectal temperature of *Cyp2e1*-null mice tended to be higher than that of WT mice ($P = 0.08$), albeit with no significant statistical difference (Fig. 1C). Furthermore, the rectal temperature of the *Cyp2e1*-null mice was markedly higher than that of the WT mice after feeding a HFD (Fig. 1D), indicating that *Cyp2e1*-null mice are protected against HFD-induced fat accumulation by increasing energy expenditure. An indirect calorimetry assay was then carried out in a 24-h cycle, and daily energy expenditure of the HFD-fed *Cyp2e1*-null mice was significantly increased over a period of 24 h (Fig. 1E). The respiratory exchange ratios of *Cyp2e1*-null mice were nearly equal to 0.7 and were significantly lower than that of WT mice (Fig. 1F), suggesting that lipid utilization was a major energy fuel for *Cyp2e1*-null mice. These results support the view that CYP2E1 deficiency increases the metabolic rate of HFD-fed mice. Thermogenesis and adipose browning were next analyzed. The expression of *Ucp1* mRNA and other thermogenesis-associated mRNAs, including cytochrome *c* oxidase subunit 8b (*Cox8b*) and PR domain containing 16 (*Prdm16*), in BAT and SWAT of *Cyp2e1*-null mice were increased (Fig. 1G and H), while the expression of these thermogenesis-associated mRNAs was not increased in EWAT (Fig. 1I), indicating selective activation of thermogenic genes in BAT and SWAT. Interestingly, histological analysis of adipose tissue from HFD-fed mice revealed a significant increase in multilobular adipocytes (Fig. 1J), a typical characteristic of beige adipocytes, in SWAT of *Cyp2e1*-null mice but not in WT mice. Furthermore, immunohistochemistry staining for UCP1 demonstrated a marked increase of UCP1 in brown-like adipocytes of SWAT from *Cyp2e1*-null mice (Fig. 1K). However, no significant difference in body weight was found in chow diet-fed mice (Fig. S1J). These data indicate that CYP2E1 deficiency induces adipose browning and enhances energy expenditure to improve obesity under HFD feeding.

3.2. Global transcriptome analysis demonstrates the correlation between CYP2E1 and PPARα pathway

To explore the potential mechanism that accounts for the metabolic phenotype, RNA-seq of hepatic mRNA in *Cyp2e1*-null and WT mice was performed. An average of 14,530 genes were detected per sample. Differential expression genes were screened with a fold change > 1.5 and P value < 0.05. Compared with WT mice, 39 differentially expressed genes were detected in *Cyp2e1*-null mice, including 29 up-regulated genes and 10 down-regulated genes (Fig. 2A and B). Among these genes, the expression of the PPARα target gene *Cyp4a10*, *Cyp4a14* and *Cyp4a31* mRNAs were significantly increased in *Cyp2e1*-null mice compared to WT mice (Fig. 2B). Distribution of the differentially expressed genes were then annotated using Gene ontology enrichment analyses and KEGG databases. Gene ontology enrichment analyses showed that these genes were enriched in "metabolic process" (Fig. 2C). KEGG pathway analyses also revealed that these differentially expressed genes mainly enriched in "metabolism" process, especially in the "lipid metabolism" pathway (Fig. 2D). To search for

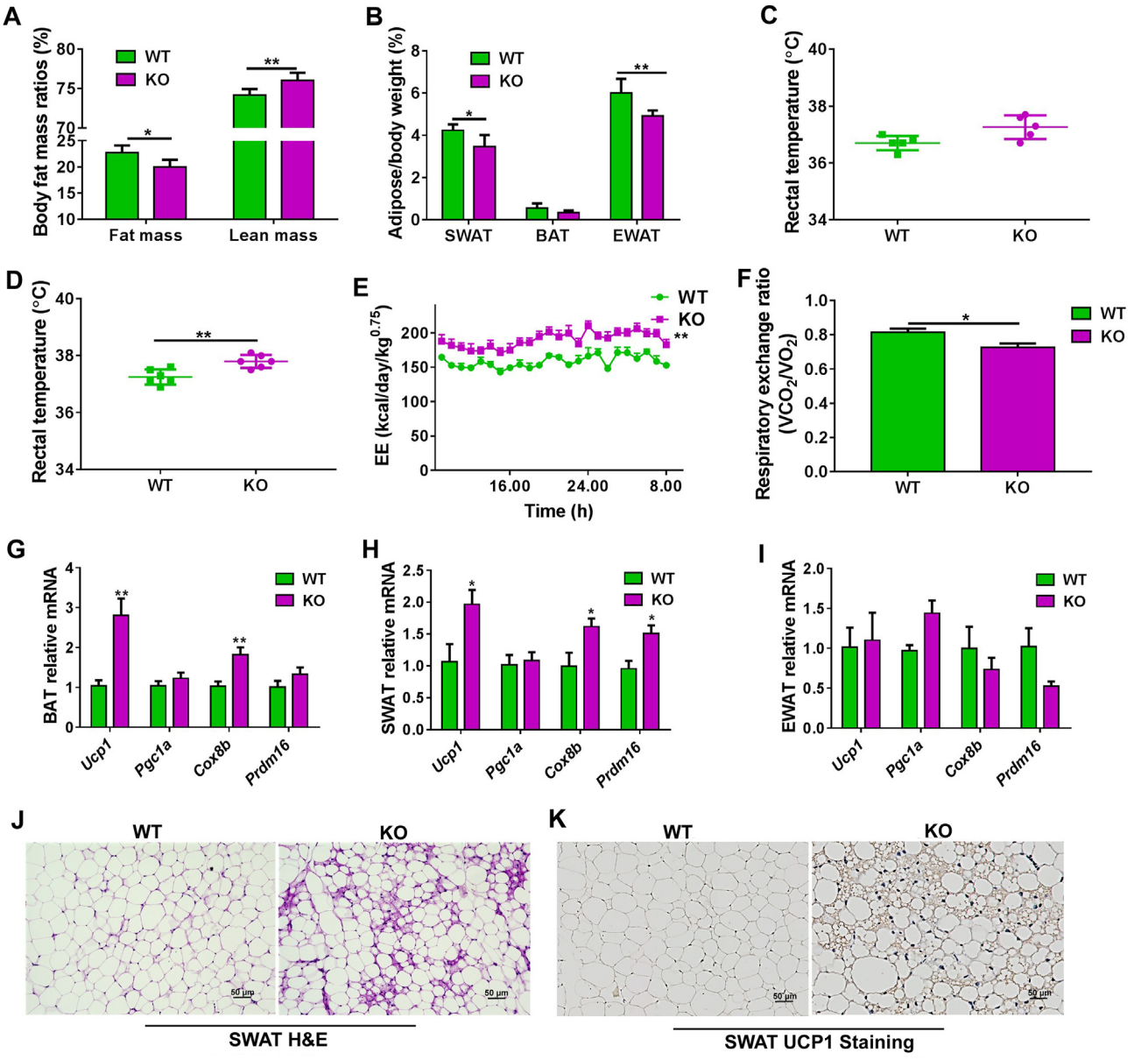

Figure 1 *Cyp2e1* disruption improves high-fat diet (HFD)-induced metabolic syndrome and increases energy expenditure. (A) Fat mass. (B) Adipose tissue/body weight ratios. (C) Circadian rectal temperature on normal condition. (D) Circadian rectal temperature after 14-week HFD feeding. (E) Daily energy expenditure (EE), data are expressed as adjusted means based on body weight to the power 0.75. (F) Respiratory exchange ratio (VCO_2/VO_2), VO_2, oxygen consumption; VCO_2, carbon dioxide production. (G–I), mRNA expression of the thermogenesis genes in brown adipose tissue (BAT), subcutaneous white adipose tissue (SWAT), and epididymal white adipose tissue (EWAT). (J, K) Representative hematoxylin and eosin (H&E) staining (J) and uncoupling protein 1 (UCP1) immunohistochemical staining (K) of SWAT sections from wild-type (WT) and *Cyp2e1*-null mice, scale bar = 50 μm. All data are presented as mean ± SEM, $n = 6$ mice/group; $^*P < 0.05$, $^{**}P < 0.01$ and $^{***}P < 0.001$, compared with WT mice group, by unpaired two-tailed *t* test. WT, wild-type. KO, knockout. SWAT, subcutaneous white adipose tissue. BAT, brown adipose tissue. EWAT, epididymal white adipose tissue.

the hub genes among these differentially-expressed genes, a gene–gene interaction network was constructed using STRING database. The results showed that 19 genes were selected for the network conduction. Among them, *Cyp2e1* gene expression was negatively correlated with that of *Cyp4a10* and *Cyp4a14,* both of which are encoded by PPARα target genes (Fig. 2E). These data reveal a potential mechanistic link where CYP2E1 deficiency results in activation of hepatic PPARα.

3.3. CYP2E1 deficiency activates PPARα–FGF21 axis and decreases hepatic lipid accumulation

The mRNA expression of PPARα target genes were then quantified. *Cyp4a10*, acyl-CoA thioesterase 1 (*Acot1*), acyl-CoA oxidase 1 (*Acox1*), carnitine palmitoyl transferase 1b (*Cpt1b*), carnitine palmitoyl transferase 2 (*Cpt2*), enoyl-CoA, hydratase/3-hydroxyacyl CoA dehydrogenase (*Ehhadh*), and *Fgf21* mRNAs

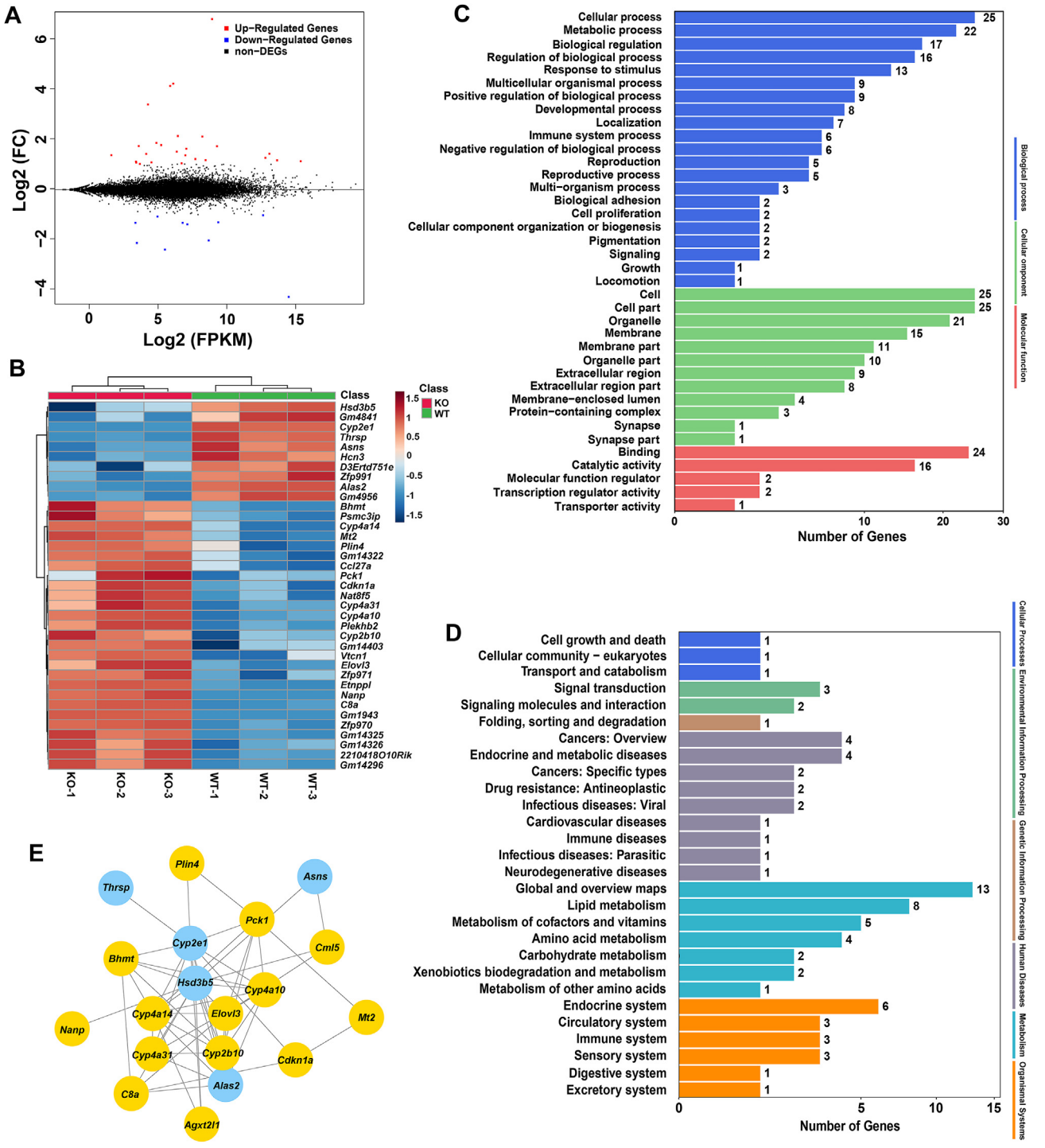

Figure 2 Transcriptome profiles revealed differential genes expression of the wild-type (WT) and *Cyp2e1-null* (KO) mice. (A) MA plot of differential gene expression levels in the two groups, where expression intensity is on the *x*-axis and differences in the gene expression levels (fold change, FC) are on the *y*-axis ($\log_2$ FC), each dot represents one gene, red dots represent genes whose abundance is significantly up-regulated, blue dots represent down-regulated, and black dots represent non-significantly changed genes. (B) Heatmap of differential gene expression in WT and KO mice. (C) Gene ontology annotation of the differentially expressed unigenes. (D) KEGG annotation of the differentially expressed unigenes. (E) Gene−gene interaction network to show the key genes that link with *Cyp2e1*. WT, wild-type. KO, knockout. FC, fold change. FPKM, fragments per kilobase million.

were all significantly increased in *Cyp2e1*-null mice compared to WT mice (Fig. 3A). Activation of PPARα increases expression of *Fgf21* encoding FGF21, a hepatokine that is released from the liver to the circulation as an endocrinal signal to modulate thermogenic gene expression and mediate non-shivering thermogenesis[32]. Serum FGF21 protein was found to be significantly higher

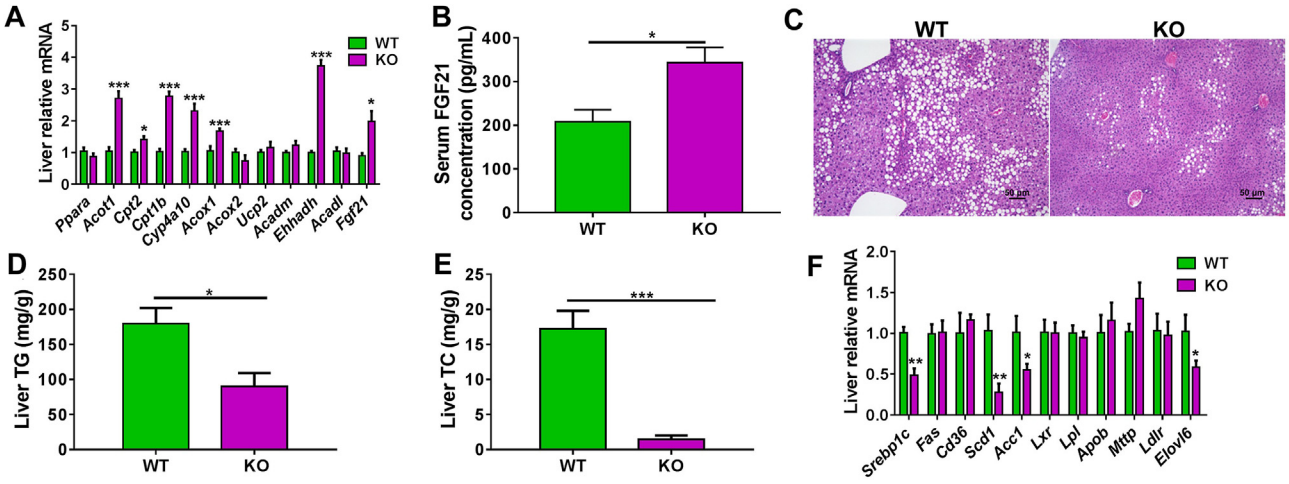

Figure 3 *Cyp2e1* disruption induced white adipose beige *via* the PPARα−FGF21 axis. (A−F) wild-type (WT) and *Cyp2e1-null* (KO) mice were fed a HFD for 14 weeks. (A) Hepatic mRNA expression of PPARα target genes under high-fat diet (HFD). (B) Serum FGF21 concentrations. (C) Representative hematoxylin and eosin (H&E) staining of liver sections from WT and KO mice, scale bar = 50 μm. (D, E) Liver triglycerides (TG), total cholesterol (TC). (F) Hepatic expression of mRNAs encoded by hepatic lipogenesis-related genes. All data are presented as mean ± SEM, $n = 6$; $^{*}P < 0.05$, $^{**}P < 0.01$ and $^{***}P < 0.001$ by unpaired two-tailed *t* test. WT, wild-type. KO, knockout.

in *Cyp2e1*-null mice than in WT mice (Fig. 3B), which likely accounts for the upregulation of thermogenic genes in BAT and SWAT and the browning of SWAT adipocytes as well as the increased energy expenditure in mice.

Hepatic PPARα activation plays a key role in restricting hepatic lipid accumulation[33]. Accordingly, histological analysis revealed less hepatic accumulation of intracellular lipid droplets in *Cyp2e1*-null mice than in WT mice (Fig. 3C). Biochemical analyses showed that hepatic TG and TC levels in *Cyp2e1*-null mice were much lower than that in WT mice (Fig. 3D and E), while no significant change was found between the two genotypes under a chow diet (Fig. S1K and S1L). The hepatic lipogenesis gene mRNAs, sterol regulatory element-binding transcription factor 1c (*Srebp1c*), stearoyl-CoA desaturase 1 (*Scd1*), acetyl-CoA carboxylase 1 (*Acc1*), and elongation of very long chain fatty acids family member 6 (*Elovl6*), were all decreased in *Cyp2e1*-null mice compared to WT mice (Fig. 3F).

3.4. Global metabolomics revealed a novel CYP2E1 endogenous substrate

Cyp2e1 disruption did not affect *Ppara* mRNA level but induced PPARα target gene expression, suggesting that endogenous PPARα agonists might be increased when CYP2E1 was inactive. To further explore which endogenous metabolites potentially mediated hepatic PPARα activation in *Cyp2e1*-null mice, LC−MS/MS-based global untargeted metabolomics were performed on liver samples obtained from HFD-fed WT and *Cyp2e1*-null mice. PCA modeling displayed an obvious separation between the two groups (Fig. 4A). A heatmap was produced for ions that were responsible for the separation of the two groups (Fig. 4B). Among the 19 ions that were upregulated in HFD-fed *Cyp2e1*-null mice, four ions ranked among the top of the list were selected for further study based on their structural similarities with published CYP2E1 substrates and PPARα agonists. By comparing their MS/MS data with that of authentic standards, these four ions were further determined to be lysophosphatidylcholine (LysoPC 22:4) and three PUFAs including DHA, AA, and LCA. Among these four endogenous metabolites, whether LysoPC 22:4 was a direct substrate of CYP2E1 had never been reported, while the three PUFAs were already suggested to be metabolized by CYP2E1 in previous studies[16−20], which could serve as positive biomarker controls of the present metabolomics study. The relative quantitation of these four markers showed that they were all elevated in *Cyp2e1*-null mice compared with WT mice (Fig. 4C for LysoPC 22:4; Supporting Information Fig. S2A−S2C for DHA, AA, LCA).

The question arose whether LysoPC 22:4 and the three PUFAs, elevated in *Cyp2e1*-null mice, were direct CYP2E1 substrates. To answer this question, molecular docking analyses *in silico* was first carried out between these compounds and the human CYP2E1 protein (PDB ID: 3LC4) by using Discovery Studio 2016 (v16.1, Accelrys, San Diego, CA, USA) software. Molecular docking scores of LysoPC 22:4, DHA, AA, and LCA were 121.933, 156.76, 144.99, and 133.87, respectively. The binding modes of LysoPC 22:4, DHA, AA, and LCA with CYP2E1 are shown (Fig. 4D for LysoPC 22:4; Fig. S2D−S2F) for DHA, AA and LCA). These data showed that all four biomarkers could interact with the CYP2E1 protein. To further identify if these compounds were direct enzyme substrates of CYP2E1, the three PUFAs (DHA, AA, and LCA) were purchased commercially, while the LysoPC 22:4 was newly synthesized by the route shown in Fig. 4E. *In vitro* incubation of LysoPC 22:4, DHA, AA and LCA with recombinant human CYP2E1 was then performed. All the compounds were metabolized by recombinant CYP2E1 and their metabolites identified by LC−MS/MS (Supporting Information Fig. S3). The metabolic sites on LysoPC 22:4 were at C-7, C-10, C-13, C-16, C-22 and ester bond (Fig. 4F), DHA were at C-9, C-17, C-20 and C-21, and AA were at C-1 and C-6 to C-16, while the metabolic sites on LCA by recombinant CYP2E1 protein were at C-6 to C-10, C-16, and C-17 (Fig. S2G). Furthermore, the CYP2E1 inhibitor DDC increased the residual levels of LysoPC 22:4 compared to control vehicle (Fig. S2H), indicating that DDC inhibits metabolism of LysoPC 22:4. These results reveal that CYP2E1 directly metabolizes the LysoPC 22:4 and the three PUFAs, thus explaining why they are elevated in the

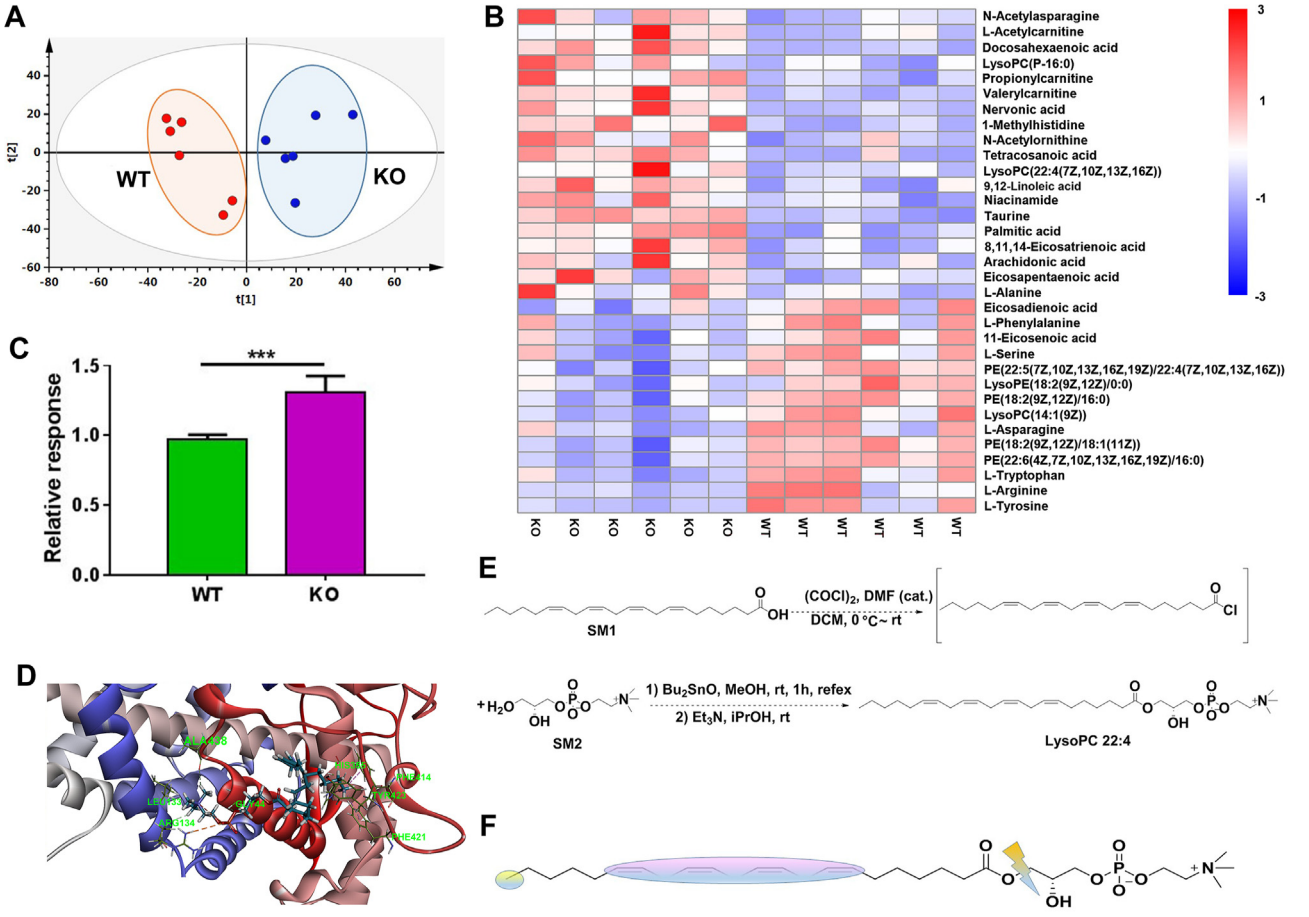

Figure 4 The LysoPC 22:4 was increased in *Cyp2e1*-null mice and identified as a direct CYP2E1 substrate. (A) Score scatter plot of a PCA model of the hepatic metabolites between wild-type (WT) and *Cyp2e1*-null (KO) mice, each point represents an individual mouse sample. (B) Heatmap analysis of the different hepatic metabolites in WT and KO mice. (C) Relative response of LysoPC 22:4 in WT and KO mice. (D) Docking pose of LysoPC 22:4 in the human CYP2E1 binding pocket. (E) Synthesis route of LysoPC 22:4. (F) Metabolic sites of LysoPC 22:4 after incubation with recombinant human CYP2E1. Data are presented as mean ± SEM, $n = 6$ mice/group; $^{***}P < 0.001$ by unpaired two-tailed *t* test. WT, wild-type. KO, knockout.

livers of *Cyp2e1*-null mice. Among these four metabolites, LysoPC 22:4 was identified as a novel CYP2E1 substrate while the other three PUFAs were systematically confirmed to be the direct CYP2E1 substrates.

3.5. *LysoPC 22:4 was identified as a novel PPARα agonist*

To determine if LysoPC 22:4 and the three PUFAs are PPARα ligands, a SPR assay was carried out to observe the interaction between Wy-14643 (a known PPARα agonist used as a positive control), LysoPC 22:4, DHA, AA, LCA, and the PPARα protein, respectively. The equilibrium binding curve fits were developed with different concentrations of these compounds, and the equilibrium dissociation constants (K_d) were calculated with Biacore T200 Evaluation Software. The extracellular binding affinity of Wy-14643, LysoPC 22:4, DHA, AA, and LCA with PPARα was 2.69, 44.5, 14.3, 16.1, and 23.8 μmol/L, respectively (Fig. 5A and B and Supporting Information Fig. S4A−S4C). Thus, the four biomarkers could serve as ligands that bind the PPARα protein.

To further determine the possible binding mode between these four biomarkers with PPARα protein, molecular docking analyses *in silico* were carried out between the three tested PUFAs and the human PPARα-ligand binding domain (LBD: aa 201−468), similarly as described[28], by using SYBYL-X 2.1.1 software. In line with the results of the SPR assay, molecular docking scores of LysoPC 22:4, DHA, AA, and LCA were 88.42, 63.58, 62.70, and 62.42, respectively, showing that LysoPC 22:4 had the strongest interaction with the PPARα protein among the four biomarkers. The binding modes of Wy-14643, LysoPC 22:4, DHA, AA, and LCA with PPARα are shown in Fig. 5C, D and Fig. S4D−S4F. To show the interaction between the ligands and PPARα protein more intuitively, eyelash maps were also created (Supporting Information Fig.S5). The interaction of Wy-14643 with PPARα was shown in Fig. S5A as a positive control, Wy-14643 showed hydrogen bond interactions with Cys276 and Phe273, carbon−hydrogen interaction with His440, alkyl interaction with Ile317, Leu321, and Met355, donner−donner interaction with Ser280, van der Waals interaction with Gln277 and Thr279, pi−alkyl interaction with Cys276, Phe318, Leu321, Ile354, Met330 and Met355, and pi−sulfur interaction with Cys276 and His440 of PPARα (Fig. S5A). The eyelash maps demonstrated that interaction of LysoPC 22:4 with PPARα was through mainly hydrophobic interactions. The lipid chain and glycerophosphate choline moieties form carbon−hydrogen interaction with Asn219,

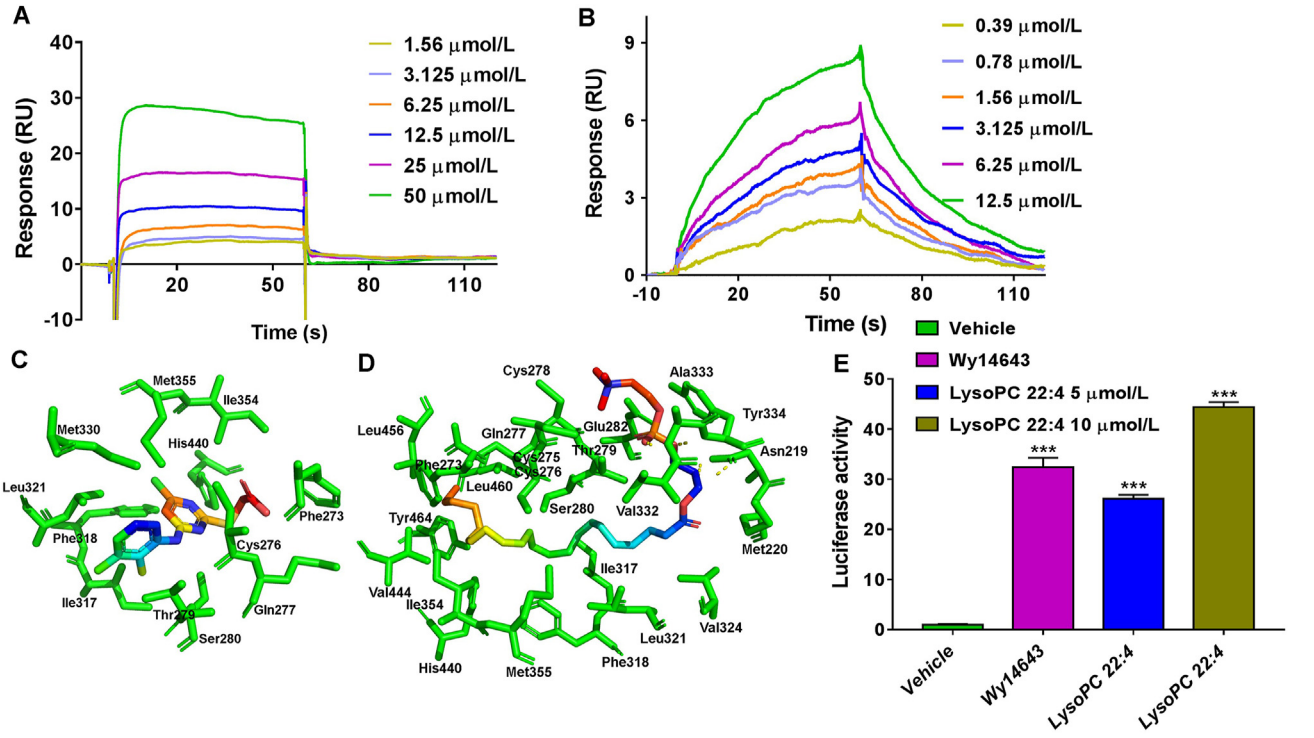

Figure 5 The LysoPC 22:4 was identified as a direct PPARα agonist. (A, B) Surface plasmon resonance (SPR) assay for interaction of Wy-14643 and LysoPC 22:4 with PPARα protein. (C, D) Docking pose of Wy-14643 and LysoPC 22:4 in the human PPARα-AF-2 binding pocket. (E) Luciferase assays for PPARα activation in HEK293 cells after treatment with 10 μmol/L Wy-14643, and 5 and 10 μmol/L LysoPC 22:4, respectively. ***$P < 0.001$, compared with vehicle group, by one-way ANOVA analysis. Data are presented as mean ± SEM; $n = 3$ per group. RU, response units.

Cys275, Thr279, Glu282 and Ala333, van der Waals interaction with Met220, Gln277, Cys278, Ser280, Val324 and Val332, negative−negative interaction with Glu282, charge−charge interaction with Glu282, alkyl interaction with Cys276, Ile317, Ile354, Met355, Val444, Leu456, Leu460 and Leu321, pi−anion interaction with Tyr334, and pi−alkyl interaction with Phe273, Phe318, His440 and Tyr464 of PPARα, separately. It can also form hydrogen bond interactions with Tyr334 and Asn219 of PPARα (Fig. S5B).

DHA binding to PPARα was mainly through hydrophobic interactions and interaction of the oxygen atom on the carbonyl group with Asn219, Glu282 and Tyr334 of PPARα to form hydrogen bonds. It also can form van der Waals interaction with Gln277, Thr279, Ser280 and Leu331 of PPARα. The hydrophobic interaction sites of PPARα with the lipid chain of DHA were shown as Met220, Tyr314, Cys276, Phe318, Ile317, His440, Leu321, Tyr334, Val324, Ile354, Met355, Tyr314, Phe318, His440 and Tyr334 (Fig. S5C). For AA binding to PPARα, the oxygen atom on the AA carbonyl group interacted with Asn219 and Glu282 to form hydrogen bonds, while the hydroxyl group also interacted with Tyr334 to form hydrogen bonds. It also can form van der Waals interaction with Thr279 and Ser280 of PPARα. The lipid chain of AA hydrophobically interacted with Met355, His440, Cys276, Phe318, Ile354, Lys358, Leu321, Ile317, Met330, Met220, Val324 and Leu331 of the PPARα protein (Fig. S5D). Similarly, the binding mode between LCA and PPARα was also through hydrophobic interactions. The lipid chain of LCA had hydrophobic interactions with Cys276, Ile317, Leu321, Val324, Met330 and Tyr334 of PPARα. The oxygen atoms on the carbonyl group interacted with Asn219 and Glu282 of PPARα to form hydrogen bonds, while the hydroxyl group interacted with Tyr334 to form hydrogen bond (Fig. S5E). These data further demonstrate the binding modes between these four biomarkers and PPARα protein.

To determine if LysoPC 22:4 and the three PUFAs also serve as PPARα agonists, transactivation of PPARα was first examined using a dual luciferase reporter assay for LysoPC 22:4, DHA, AA and LCA with Wy-14643 as a positive control. These compounds significantly activated PPARα in HEK-293 cells, and LysoPC 22:4 showed the most potent activity among the four biomarkers, which was even higher than the positive control Wy-14643 when used at 10 μmol/L, suggesting that LysoPC 22:4 is a novel potent endogenous PPARα agonist (Fig. 5E and Fig. S4G). These data further support the view that these four biomarkers are the direct agonists of PPARα, among which LysoPC 22:4 is a novel potent PPARα agonist.

3.6. CYP2E1-specific antagonist induces adipose browning and alleviates obesity via the PPARα−FGF21 axis

To verify whether CYP2E1 could be a pharmacotherapy target for treating obesity and its associated metabolic syndrome, HFD-fed WT mice were intraperitoneally administered PBS or 40 mg/kg of DDC, a CYP2E1 inhibitor. DDC treatment substantially inhibited HFD-induced body weight gain and improved glucose tolerance and insulin resistance of mice compared with PBS treatment (Fig. 6A−C). Histology analysis showed that DDC reduced hepatic lipid accumulation, induced browning of SWAT, and increased UCP1 protein expression in SWAT compared with the PBS treatment (Fig. 6D and E). The mRNA expression of the

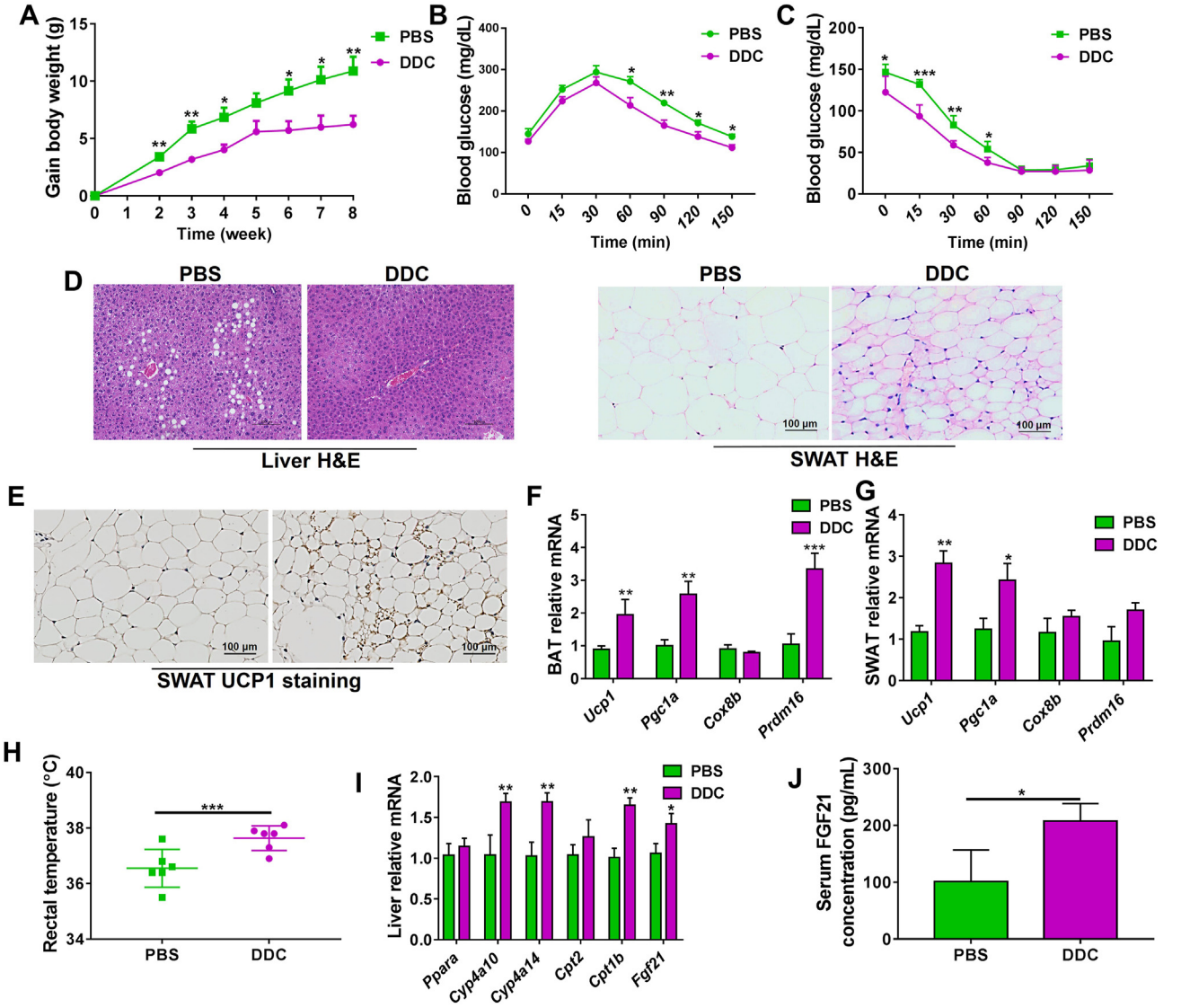

Figure 6 CYP2E1 antagonist alleviates high-fat diet-induced obesity *via* PPARα−FGF21−beige axis. (A) Body weight gain. (B) Glucose tolerance test. (C) Insulin tolerance test. (D) Representative hematoxylin and eosin (H&E) staining of liver and subcutaneous white adipose tissue (SWAT) sections from phosphate buffered saline (PBS) and diethyldithiocarbamate (DDC)-treated mice, scale bar = 100 μm. (E) Representative uncoupling protein 1 (UCP1) immunohistochemical staining (right) of subcutaneous white adipose tissue (SWAT) sections from PBS and DDC-treated mice, scale bar = 100 μm. (F, G) mRNA expression of the thermogenesis genes in brown adipose tissue (BAT) and SWAT. (H) Rectal temperature. (I) Hepatic mRNA expression of PPARα target genes. (J) Serum FGF21 concentrations. Data are presented as mean ± SEM, $n = 6$; $^{*}P < 0.05$; $^{**}P < 0.01$ and $^{***}P < 0.001$ by unpaired two-tailed t test.

thermogenesis genes *Ucp1*, *Pgc1a*, and *Prdm16* in BAT, and *Ucp1*, and *Pgc1a* in SWAT were increased by DDC treatment in WT mice (Fig. 6F and G). Similar with the observations in HFD-fed *Cyp2e1*-null mice, DDC-treated WT mice exhibited higher rectal temperature (Fig. 6H), lower weights of liver and white adiposes, and lower levels of hepatic TG and TC levels compared to PBS-treated mice (Supporting Information Fig. S6A−S6E). In HFD-fed WT mice, DDC decreased serum TC levels in the absence of changes in serum TG levels (Fig. S6F and S6G). DDC treatment significantly decreased the serum AST levels, while tended to decrease the serum ALT levels (Fig. S6H and S6I). Accordingly, the mRNA levels of PPARα target genes including *Cyp4a10*, *Cyp4a14, Cpt1b* and *Fgf21* were increased in the livers of DDC-treated WT mice (Fig. 6I). In addition, serum FGF21 levels in DDC-treated mice were higher than in PBS-treated WT mice (Fig. 6J). Thus, consistent with genetic CYP2E1 ablation, CYP2E1 antagonism by DDC decreased the obesity accompanied by induced hepatic PPARα−FGF21 activation and induced white adipose browning.

While DDC has a marked anti-obesity effect in HFD-fed mice, DDC failed to further decrease the body weight and also showed no effect in white adipose weight and liver weight in the matched HFD-fed *Cyp2e1*-null mice (Supporting Information Fig. S7A−S7D). Accordingly, DDC showed no significant effect in HFD-induced liver TG and TC accumulation as well as the rectal temperature (Fig. S7E−S7G). Hepatic PPARα activation and SWAT thermogenesis were also abolished in *Cyp2e1*-null mice (Fig. S7H and S7I). These data demonstrate that the anti-

obesity effect of DDC was lost in *Cyp2e1*-null mice, supporting an on-target effect of this CYP2E1 inhibitor for the treatment of metabolic disorders.

3.7. *Anti-obesity effect of CYP2E1 inhibitor depends on the presence of hepatic PPARα*

To explore whether hepatic PPARα activation is a result or a cause of improved metabolic disorders in CYP2E1-inhibited mice, HFD-treated *Ppara*$^{\Delta Hep}$ mice were intraperitoneally administered PBS or 40 mg/kg of DDC once daily for 8 weeks, and mouse weights recorded once a week. DDC failed to affect HFD-induced body-weight gain, white adipose weights, insulin resistance and rectal temperature in *Ppara*$^{\Delta Hep}$ mice (Fig. 7A−F). In addition, no difference of hepatic mRNA expression for the PPARα target genes including *Fgf21* was noted in livers of DDC-treated and PBS-treated *Ppara*$^{\Delta Hep}$ mice (Fig. 7G). Accordingly, the effects of DDC on inducing the mRNA levels of the thermogenesis genes in the BAT and SWAT were lost in *Ppara*$^{\Delta Hep}$ mice (Fig. 7H and I). No notable changes of serum FGF21 levels by DDC treatment were found in HFD-treated *Ppara*$^{\Delta Hep}$ mice (Fig. 7J). Histological analyses showed that hepatic lipid levels and adipocyte size as well as UCP1 expression in SWAT were not changed by DDC treatment (Fig. 7K and L). Biochemical analyses showed no notable change of hepatic TG/TC, serum TG/TC and serum ALT/AST levels (Fig. 7M−R). All the above findings reveal that the improvement of obesity-associated disorders by CYP2E1 antagonism is lost in *Ppara*$^{\Delta Hep}$ mice.

4. Discussion

Although CYP2E1 as the metabolic enzyme and PPARα as the metabolic nuclear receptors are well-known to modulate metabolic homeostasis, whether and how CYP2E1 inhibition could be a method to induce white adipose browning by crosstalk with PPARα *via* sharing the same endogenous compounds as enzyme substrates and agonists have not been explored. Here, a novel CYP2E1−PPARα crosstalk was revealed to modulate adipose browning. CYP2E1 could be directly targeted by use of the chemical inhibitor DDC for the therapeutic treatment of obesity and inducing adipose browning. Mechanically, CYP2E1-mediated hepatic PPARα activation was probably due to the increase of LysoPC 22:4, DHA, AA and LCA, in *Cyp2e1*-null mice, and these biomarkers were further demonstrated to be both enzyme substrates of CYP2E1 and direct PPARα agonists, among which LysoPC 22:4 was identified as a novel endogenous CYP2E1 enzyme substrate and a new potent endogenous PPARα agonist. A schematic of the proposed mechanism that accounts for the major findings in this study is shown in Fig. 8. In line with the "multiple organ−multiple hits model" for the pathological progression mechanism of nonalcoholic fatty liver disease proprosed previously[34], the current study further supports the potential of liver-adipose crosstalk in modulating obesity and fatty liver.

Recent studies have focused on the regulation of non-shivering thermogenesis for the treatment of obesity[35,36]. However, it is largely unknown whether targeting metabolic enzymes such as CYP2E1, that is largely known for catalyzing xenobiotic-metabolism[15], modulates thermogenic adipose browning. A striking finding from this study is that CYP2E1 deficiency activates the white adipose browning, accompanied by increased core temperature and energy expenditure. Various methods were developed to activate white adipose browning such as the voluntary intermittent fasting[27] and intestinal farnesoid X receptor[37] or hypoxia-inducible factor 2α[31] antagonism, cold exposure[38] and β-adrenergic receptor agonism[39,40]. However, brown adipocyte activation by cold exposure and β-adrenergic receptor agonism is clinically non-feasible, while long-term intermittent fasting could be intolerant for many people. Understanding the underlying mechanisms how CYP2E1 functional loss drives white adipose browning could reveal new alternative pharmacotherapies.

Implicit of the mechanistic link between CYP2E1 deficiency and white adipose browning is that CYP2E1 deficiency activates the PPARα−FGF21 axis. FGF21, encoded by a PPARα target gene[12], was shown to be involved in white adipose browning[32,41], and FGF21 modulators or analogues have emerged as promising anti-obesity therapies both in rodent models and humans[42,43]. Hepatic PPARα activation induced by CYP2E1 deficiency increased the expression and excretion of FGF21 from liver, which circulates to induce the remote adipose tissue browning. This finding supports the possibility that inhibition of CYP2E1 could activate PPARα and modulate FGF21 release. In line with the present findings, a previous study also demonstrates the CYP4A enzymes, encoded PPARα target genes, are activated in livers of *Cyp2e1*-null mice during acute acetaminophen-induced liver injury[44]. In addition to enhanced FGF21 release, CYP2E1 deficiency also markedly induced the expression of genes involved in fatty acid β-oxidation such as *Acox1*, *Acot1*, *Cpt2*, *Ehhadh*, *Acot1*, all of which are typical PPARα target genes; activation of these β-oxidation-related genes is concurrent with the marked activation of PPARα induced by CYP2E1 disruption. Beyond PPARα activation, the anti-obesity effects of CYP2E1 deficiency were also accompanied by decreased hepatic lipogenesis. A recent study using E3 ubiquitin ligase knockout mouse models to elevate hepatic CYP2E1 levels, found that increased hepatic CYP2E1 alone was insufficient to promote the progression of nonalcoholic fatty liver disease under chow diet feeding due to lack of concurrent hepatic lipogenesis or increased dietary lipids, suggesting that CYP2E1 does not directly modulate lipogenesis[45]. Thus, decreased hepatic lipogenesis under HFD in *Cyp2e1*-null mice is possibly a result of *CYP2E1* gene deficiency-induced lower obesity.

The increased LysoPC 22:4 and three PUFAs were further identified to mediate the mechanism of CYP2E1 deficiency-induced hepatic PPARα activation as signaling-transducing molecules. PPARα is nuclear receptor that can be modulated by endogenous ligands[21−23]. Intriguingly, global metabolomics screening found that function loss of CYP2E1 resulted in a significant increase of LysoPC 22:4 and three PUFAs, DHA, AA and LCA in the liver, the same tissue where PPARα is highly expressed that could regulate hepatic FGF21 release once activated. These biomarkers were further validated to function as both CYP2E1 enzyme substrates and direct PPARα agonists. Once CYP2E1 is inhibited, liver-mediated metabolism of endogenous metabolites of CYP2E1 including LysoPC 22:4, DHA, AA and LCA is blunted so that these compounds are increased in hepatocytes, which then act as the direct PPARα agonists to induce orthotopic hepatocyte activation. Notably, LysoPC 22:4 was synthesized and verified as a newly-described CYP2E1 substrate and PPARα agonist.

Another important finding from the present study is that the CYP2E1 inhibitor DDC causes marked white adipose browning and attenuates metabolic dysfunction depending on the presence of hepatic PPARα. The causal relationship for the contribution of

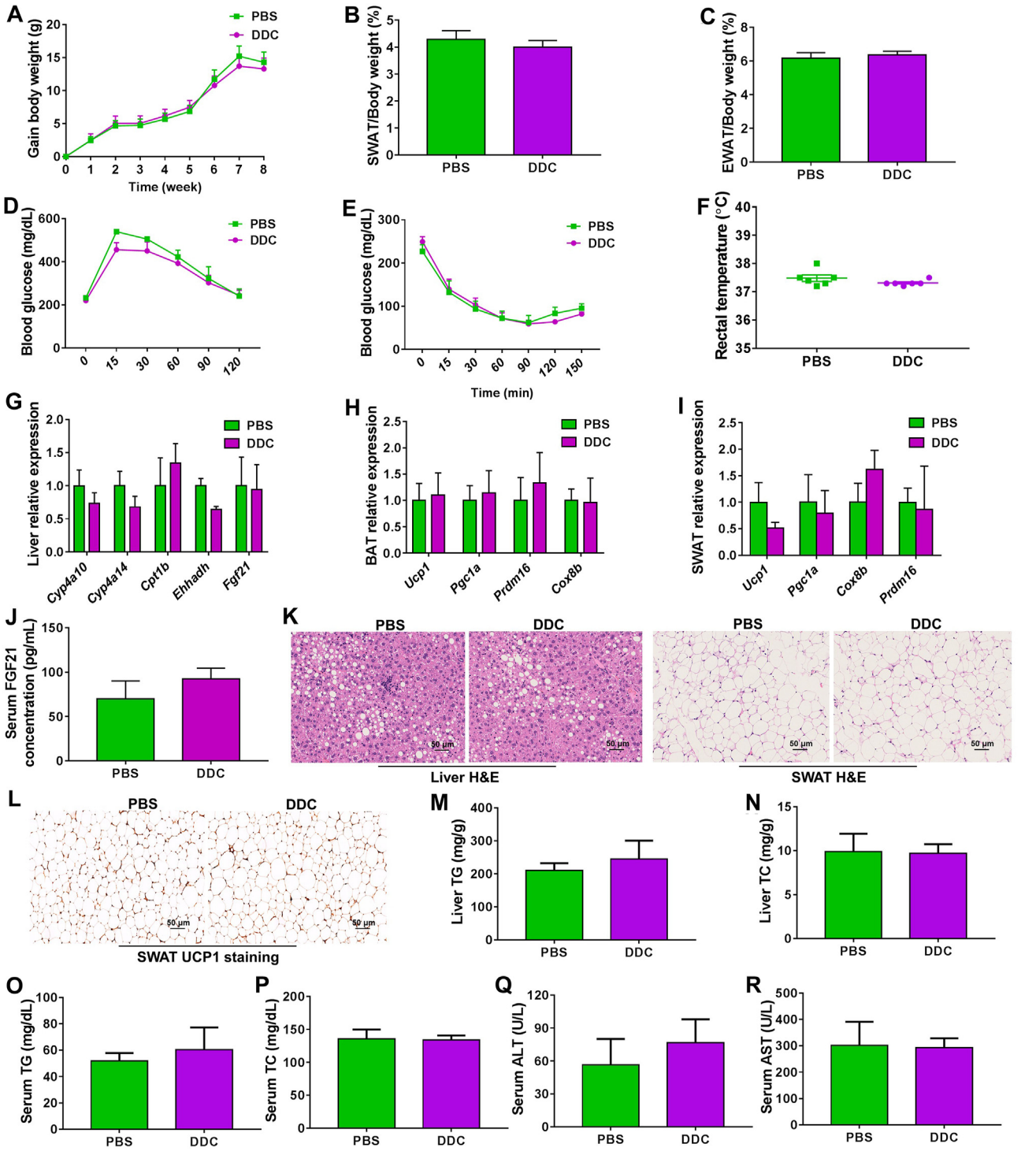

Figure 7 Anti-obesity effect of *Cyp2e1* inhibition is lost in the absence of liver PPARα. (A) Body weight gain. (B) Subcutaneous adipose tissue (SWAT)/body weight ratio. (C) Epididymal adipose tissue (EWAT)/body weight ratio. (D) Glucose tolerance test. (E) Insulin tolerance test. (F) Rectal temperature. (G) Hepatic mRNA expression of PPARα target genes. (H, I) mRNA expression of the thermogenesis genes in brown adipose tissue (BAT) and SWAT. (J) Serum FGF21 concentration. (K) Representative hematoxylin and eosin (H&E) staining of liver and subcutaneous white adipose tissue (SWAT) sections from phosphate buffered saline (PBS) and diethyldithiocarbamate (DDC)-treated mice, scale bar = 50 μm. (L) Representative uncoupling protein 1 (UCP1) staining of SWAT. (M) Liver triglycerides (TG). (N) Liver total cholesterol (TC). (O) Serum TG. (P) Serum TC. (Q) Serum alanine transaminase (ALT) levels. (R) Serum aspartate transaminase (AST) levels. Data are presented as mean ± SEM, $n = 6$.

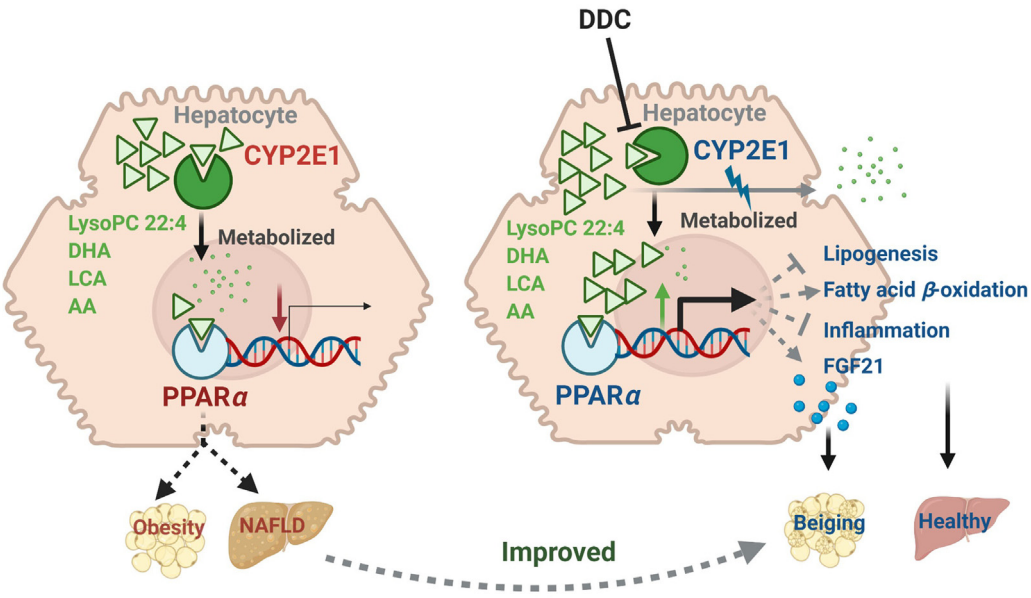

Figure 8 Proposed CYP2E1−PPARα−FGF21 axis in inducing white adipose browning for reducing obesity. CYP2E1 deficiency, either by gene disruption or chemical inhibition, leads to hepatic PPARα activation that decreases lipid accumulation as well as increasing the expression and secretion of FGF21 from the liver. Secreted FGF21 then circulates to the peripheral subcutaneous white adipose to enhance beiging, which in turn increases the energy expenditure and decreases obesity.

hepatic PPARα activation to the anti-obesity effects of DDC was validated using liver-specific *Ppara*-null mice. The CYP2E1 inhibitor induced white adipose browning and improved obesity to a marked extent *via* the PPARα−FGF21 axis only in HFD-fed WT mice, but not in liver-specific *Ppara*-null mice, demonstrating that CYP2E1 deficiency-mediated hepatic PPARα activation is a cause but not a result that could contribute to its anti-obesity effect. Since CYP2E1 is predominantly expressed in hepatocytes where metabolism mainly occurs, targeted inhibition of CYP2E1 could possibly achieve the PPARα activation in the orthotopic hepatocytes, which could avoid the side-effects of non-tissue-specific PPARα activation that happens occasionally in clinic[46].

By taking advantage of the shared structural similarities between CYP2E1 substrates and PPARα agonists, the present work uncovered novel perspectives on beige-fat development by CYP2E1 inhibition *via* a crosstalk with PPARα, providing a novel druggable target for adipose browning induction. Crosstalk between metabolic enzymes and nuclear receptors by sharing the same substrates as singling-transducing molecules deserves additional studies. Notably, natural products such as resveratrol, quercetin, myricetin, are known as dietary CYP2E1 inhibitors[47,48], that are present in many dietary sources such as red wine, coffee and fruits[49,50]. Based on results of the current study, CYP2E1 inhibition by these natural products may partially explain their beneficial effects in restricting obesity-associated metabolic syndrome and fatty liver[34,51,52]. CYP2E1 inhibition could potentially be a pharmacological target. For example, disulfiram, an FDA-approved drug treatment for alcoholism, was reported to have a potent anti-obesity effect which is not through its inhibitory effects on aldehyde dehydrogenase 2 (ALDH2)[53]. Structurally, disulfiram could be metabolized into DDC[54], the CYP2E1 inhibitor[24], and thus it is reasonable to infer that the effect of disulfiram is possibly through its metabolite DDC-mediated CYP2E1 inhibition.

5. Conclusions

In the present study, by combined use of global genomics and metabolomics with *Cyp2e1*-null mice and hepatocyte-specific PPARα knockout mice, a novel crosstalk between CYP2E1and PPARα that modulates adipose browning and obesity was established with their shared substrates, LysoPC 22:4, DHA, AA and LCA as the signaling-transducing molecules, among which LysoPC 22:4 is a novel endogenous substrate of CYP2E1 that also serves as a novel bona fide PPARα agonist. Genetic CYP2E1 ablation causes an increase of its endogenous PUFA substrates, which subsequently serve as endogenous PPARα agonists. Hepatic PPARα activation results in induced expression of its target genes and FGF21 release, which then enhances remote white adipose beiging leading to a reduced obesity-associated metabolic syndrome. Treatment with a CYP2E1 inhibitor DDC also alleviates the obesity-associated metabolic syndrome by inducing the activation of PPARα−FGF21 axis and adipose browning depending on the presence of hepatocyte PPARα. These findings define the CYP2E1−PPARα axis as a novel therapeutic target for obesity treatment.

Acknowledgments

We thank Linda G. Byrd for the animal protocols submission and Oksana Gavrilova for assistance with energy expenditure experiments. We thank Meiqi Wan, Lei Zhang, Aihong Zhao, Guolin Li, Jiang Yue, Qiao Wang, Xiaoxia Gao, Yuhong Luo, Lei Chen, Tomoki Yagai, Chad N. Brocker, and Weiwei Liu for help with the mouse studies. We thank Wen Ma and Jun Li for help with LC−MS/MS experiments. This work was funded by National Cancer Institute Intramural Research Program and the National Natural Science Foundation of China (81891011).

Author contributions

Conceptualization: Tingting Yan, Youbo Zhang and Frank J. Gonzalez; Investigation: Youbo Zhang, Tingting Yan, Tianxia Wang, Xiaoyan Liu, Keisuke Hamada, Dongxue Sun, Yizheng Sun, Yanfang Yang, Jing Wang, Shogo Takahashi, Qiong Wang; Methodology: Youbo Zhang, Tingting Yan, Kristopher W. Krausz, Changtao Jiang, Cen Xie; Writing-original draft: Youbo Zhang and Tingting Yan; Writing-review and editing: Tingting Yan, Youbo Zhang and Frank J. Gonzalez; Funding acquisition: Frank J. Gonzalez and Xiuwei Yang; Project administration: Tingting Yan, Youbo Zhang, Frank J. Gonzalez; Supervision: Frank J. Gonzalez, Tingting Yan, Youbo Zhang and Xiuwei Yang.

Conflicts of interest

The authors declared no competing conflict of interest.

Appendix A. Supporting information

Supporting data to this article can be found online at https://doi.org/10.1016/j.apsb.2022.02.004.

References

1. Bluher M. Obesity: global epidemiology and pathogenesis. *Nat Rev Endocrinol* 2019;**15**:288−98.
2. Kurylowicz A, Puzianowska-Kuznicka M. Induction of adipose tissue browning as a strategy to combat obesity. *Int J Mol Sci* 2020;**21**:6241.
3. Shi Y, Burn P. Lipid metabolic enzymes: emerging drug targets for the treatment of obesity. *Nat Rev Endocrinol* 2004;**3**:695−710.
4. De Bosscher K, Desmet SJ, Clarisse D, Estebanez-Perpina E, Brunsveld L. Nuclear receptor crosstalk-defining the mechanisms for therapeutic innovation. *Nat Rev Endocrinol* 2020;**16**:363−77.
5. Wang Z, Hall SD, Maya JF, Li L, Asghar A, Gorski JC. Diabetes mellitus increases the *in vivo* activity of cytochrome P450 2E1 in humans. *Br J Clin Pharmacol* 2003;**55**:77−85.
6. O'Shea D, Davis SN, Kim RB, Wilkinson GR. Effect of fasting and obesity in humans on the 6-hydroxylation of chlorzoxazone: a putative probe of CYP2E1 activity. *Clin Pharmacol Ther* 1994;**56**:359−67.
7. van Rongen A, Valitalo PAJ, Peeters MYM, Boerma D, Huisman FW, van Ramshorst B, et al. Morbidly obese patients exhibit increased CYP2E1-mediated oxidation of acetaminophen. *Clin Pharmacokinet* 2016;**55**:833−47.
8. Yoo JS, Ning SM, Pantuck CB, Pantuck EJ, Yang CS. Regulation of hepatic microsomal cytochrome P4502E1 level by dietary lipids and carbohydrates in rats. *J Nutr* 1991;**121**:959−65.
9. Zong H, Armoni M, Harel C, Karnieli E, Pessin JE. Cytochrome P-450 CYP2E1 knockout mice are protected against high-fat diet-induced obesity and insulin resistance. *Am J Physiol Endocrinol Metab* 2012;**302**:E532−9.
10. Abdelmegeed MA, Banerjee A, Yoo SH, Jang S, Gonzalez FJ, Song BJ. Critical role of cytochrome P450 2E1 (CYP2E1) in the development of high fat-induced non-alcoholic steatohepatitis. *J Hepatol* 2012;**57**:860−6.
11. Laeger T, Henagan TM, Albarado DC, Redman LM, Bray GA, Noland RC, et al. FGF21 is an endocrine signal of protein restriction. *J Clin Invest* 2014;**124**:3913−22.
12. Lundasen T, Hunt MC, Nilsson LM, Sanyal S, Angelin B, Alexson SEH, et al. PPARα is a key regulator of hepatic FGF21. *Biochem Biophys Res Commun* 2007;**360**:437−40.
13. Goto T, Hirata M, Aoki Y, Iwase M, Takahashi H, Kim M, et al. The hepatokine FGF21 is crucial for peroxisome proliferator-activated receptor α agonist-induced amelioration of metabolic disorders in obese mice. *J Biol Chem* 2017;**292**:9175−90.
14. Lu Y, Cederbaum AI. CYP2E1 and oxidative liver injury by alcohol. *Free Radic Biol Med* 2008;**44**:723−38.
15. Chen J, Jiang S, Wang J, Renukuntla J, Sirimulla S, Chen J. A comprehensive review of cytochrome P450 2E1 for xenobiotic metabolism. *Drug Metab Rev* 2019;**51**:178−95.
16. Fukuda T, Imai Y, Komori M, Nakamura M, Kusunose E, Satouchi K, et al. Different mechanisms of regioselection of fatty acid hydroxylation by laurate (omega-1)-hydroxylating P450s, P450 2C2 and P450 2E1. *J Biochem* 1994;**115**:338−44.
17. Laethem RM, Balazy M, Falck JR, Laethem CL, Koop DR. Formation of 19(*S*)-, 19(*R*)-, and 18(*R*)-hydroxyeicosatetraenoic acids by alcohol-inducible cytochrome P450 2E1. *J Biol Chem* 1993;**268**:12912−8.
18. Porubsky PR, Battaile KP, Scott EE. Human cytochrome P450 2E1 structures with fatty acid analogs reveal a previously unobserved binding mode. *J Biol Chem* 2010;**285**:22282−90.
19. Porubsky PR, Meneely KM, Scott EE. Structures of human cytochrome P-450 2E1. Insights into the binding of inhibitors and both small molecular weight and fatty acid substrates. *J Biol Chem* 2008;**283**:33698−707.
20. Roy U, Joshua R, Stark RL, Balazy M. Cytochrome P450/NADPH-dependent biosynthesis of 5,6-*trans*-epoxyeicosatrienoic acid from 5,6-*trans*-arachidonic acid. *Biochem J* 2005;**390**:719−27.
21. Huang JS, Jia YZ, Fu T, Viswakarma N, Bai L, Rao MS, et al. Sustained activation of PPARα by endogenous ligands increases hepatic fatty acid oxidation and prevents obesity in *ob/ob* mice. *FASEB J* 2012;**26**:628−38.
22. Hostetler HA, Petrescu AD, Kier AB, Schroeder F. Peroxisome proliferator-activated receptor α interacts with high affinity and is conformationally responsive to endogenous ligands. *J Biol Chem* 2005;**280**:18667−82.
23. Forman BM, Chen J, Evans RM. Hypolipidemic drugs, polyunsaturated fatty acids, and eicosanoids are ligands for peroxisome proliferator-activated receptors α and δ. *Proc Natl Acad Sci U S A* 1997;**94**:4312−7.
24. Pratt-Hyatt M, Lin HL, Hollenberg PF. Mechanism-based inactivation of human CYP2E1 by diethyldithocarbamate. *Drug Metab Dispos* 2010;**38**:2286−92.
25. Lee SS, Buters JT, Pineau T, Fernandez-Salguero P, Gonzalez FJ. Role of CYP2E1 in the hepatotoxicity of acetaminophen. *J Biol Chem* 1996;**271**:12063−7.
26. Brocker CN, Yue J, Kim D, Qu A, Bonzo JA, Gonzalez FJ. Hepatocyte-specific PPARA expression exclusively promotes agonist-induced cell proliferation without influence from nonparenchymal cells. *Am J Physiol Gastrointest Liver Physiol* 2017;**312**:G283−99.
27. Li G, Xie C, Lu S, Nichols RG, Tian Y, Li L, et al. Intermittent fasting promotes white adipose browning and decreases obesity by shaping the gut microbiota. *Cell Metabol* 2017;**26**:672−685.e4.
28. Egawa D, Itoh T, Akiyama Y, Saito T, Yamamoto K. 17-OxoDHA is a PPARα/γ dual covalent modifier and agonist. *ACS Chem Biol* 2016;**11**:2447−55.
29. Sun D, Gao X, Wang Q, Krausz KW, Fang Z, Zhang Y, et al. Metabolic map of the antiviral drug podophyllotoxin provides insights into hepatotoxicity. *Xenobiotica* 2021;**51**:1047−59.
30. Yan T, Wang H, Zhao M, Yagai T, Chai Y, Krausz KW, et al. Glycyrrhizin protects against acetaminophen-induced acute liver injury *via* alleviating tumor necrosis factor α-mediated apoptosis. *Drug Metab Dispos* 2016;**44**:720−31.
31. Xie C, Yagai T, Luo Y, Liang X, Chen T, Wang Q, et al. Activation of intestinal hypoxia-inducible factor 2α during obesity contributes to hepatic steatosis. *Nat Med* 2017;**23**:1298−308.
32. Geng L, Lam KSL, Xu A. The therapeutic potential of FGF21 in metabolic diseases: from bench to clinic. *Nat Rev Endocrinol* 2020;**16**:654−67.
33. Bougarne N, Weyers B, Desmet SJ, Deckers J, Ray DW, Staels B, et al. Molecular actions of PPARα in lipid metabolism and inflammation. *Endocr Rev* 2018;**39**:760−802.
34. Yan T, Yan N, Wang P, Xia Y, Hao H, Wang G, et al. Herbal drug discovery for the treatment of nonalcoholic fatty liver disease. *Acta Pharm Sin B* 2020;**10**:3−18.

35. Betz MJ, Enerback S. Targeting thermogenesis in brown fat and muscle to treat obesity and metabolic disease. *Nat Rev Endocrinol* 2018;**14**:77−87.
36. Palmer BF, Clegg DJ. Non-shivering thermogenesis as a mechanism to facilitate sustainable weight loss. *Obes Rev* 2017;**18**:819−31.
37. Jiang C, Xie C, Lv Y, Li J, Krausz KW, Shi J, et al. Intestine-selective farnesoid X receptor inhibition improves obesity-related metabolic dysfunction. *Nat Commun* 2015;**6**:10166.
38. Paschos GK, Tang SY, Theken KN, Li X, Verginadis I, Lekkas D, et al. Cold-induced browning of inguinal white adipose tissue is independent of adipose tissue cyclooxygenase-2. *Cell Rep* 2018;**24**:809−14.
39. Liu D, Bordicchia M, Zhang C, Fang H, Wei W, Li JL, et al. Activation of mTORC1 is essential for β-adrenergic stimulation of adipose browning. *J Clin Invest* 2016;**126**:1704−16.
40. de Jong JMA, Wouters RTF, Boulet N, Cannon B, Nedergaard J, Petrovic N. The β3-adrenergic receptor is dispensable for browning of adipose tissues. *Am J Physiol Endocrinol Metab* 2017;**312**:E508−18.
41. Fisher FM, Kleiner S, Douris N, Fox EC, Mepani RJ, Verdeguer F, et al. FGF21 regulates PGC-1α and browning of white adipose tissues in adaptive thermogenesis. *Genes Dev* 2012;**26**:271−81.
42. Gaich G, Chien JY, Fu H, Glass LC, Deeg MA, Holland WL, et al. The effects of LY2405319, an FGF21 analog, in obese human subjects with type 2 diabetes. *Cell Metabol* 2013;**18**:333−40.
43. Kliewer SA, Mangelsdorf DJ. A dozen years of discovery: insights into the physiology and pharmacology of FGF21. *Cell Metabol* 2019;**29**:246−53.
44. Chen C, Krausz KW, Shah YM, Idle JR, Gonzalez FJ. Serum metabolomics reveals irreversible inhibition of fatty acid β-oxidation through the suppression of PPARα activation as a contributing mechanism of acetaminophen-induced hepatotoxicity. *Chem Res Toxicol* 2009;**22**:699−707.
45. Correia MA, Kwon D. Why hepatic CYP2E1-elevation by itself is insufficient for inciting NAFLD/NASH: inferences from two genetic knockout mouse models. *Biology (Basel)* 2020;**9**:419.
46. Bugge A, Holst D. PPAR agonists, −Could tissue targeting pave the way?. *Biochimie* 2017;**136**:100−4.
47. Piver B, Berthou F, Dreano Y, Lucas D. Inhibition of CYP3A, CYP1A and CYP2E1 activities by resveratrol and other non volatile red wine components. *Toxicol Lett* 2001;**125**:83−91.
48. Ostlund J, Zlabek V, Zamaratskaia G. *In vitro* inhibition of human CYP2E1 and CYP3A by quercetin and myricetin in hepatic microsomes is not gender dependent. *Toxicology* 2017;**381**:10−8.
49. Jang H, Lee JW, Lee C, Jin Q, Lee MK, Lee CK, et al. Flavonol glycosides from the aerial parts of *Gynostemma pentaphyllum* and their antioxidant activity. *Arch Pharm Res* 2016;**39**:1232−6.
50. Soleas GJ, Diamandis EP, Goldberg DM. Wine as a biological fluid: history, production, and role in disease prevention. *J Clin Lab Anal* 1997;**11**:287−313.
51. Nabavi SF, Russo GL, Daglia M, Nabavi SM. Role of quercetin as an alternative for obesity treatment: you are what you eat. *Food Chem* 2015;**179**:305−10.
52. Imran M, Saeed F, Hussain G, Imran A, Mehmood Z, Gondal TA, et al. Myricetin: a comprehensive review on its biological potentials. *Food Sci Nutr* 2021;**9**:5854−68.
53. Bernier M, Mitchell SJ, Wahl D, Diaz A, Singh A, Seo W, et al. Disulfiram treatment normalizes body weight in obese mice. *Cell Metabol* 2020;**32**:203−214 e4.
54. Strume JH. Metabolism of disulfiram and diethyldithiocarbamate in rats with demonstration of an *in vivo* ethanol-induced inhibition of the glucuronic acid conjugation of the thiol. *Biochem Pharmacol* 1965;**14**:393−410.